JAAS

ROYAL SOCIETY OF CHEMISTRY

PAPER

View Article Online
View Journal

Check for updates

Cite this: DOI: 10.1039/c9ja00426b

Allanite U–Th–Pb geochronology by ion microprobe†

Xin Liao, [abc] Qiu-li Li, *[abc] M. J. Whitehouse, [d] Yue-heng Yang [ac] and Yu Liu [ac]

Allanite, an epidote group mineral, occurs as a common accessory mineral in igneous, metamorphic rocks and hydrothermal deposits. It contains radioactive elements Th and U, making it a valuable U–Th–Pb geochronometer for various geological processes. Due to the structural and compositional complexity of allanite, *in situ* dating method is a better choice when the allanite is heterogeneous or has crystallized in multi-stage events. The wide variation of chemical compositions, however, raises the potential for matrix effects and complicates the use of *in situ* methods for allanite U–Th–Pb chronology. To address this issue, we made a comprehensive investigation on allanite U–Th–Pb chronology using Secondary Ion Mass Spectrometry (SIMS). Five allanite samples (CAP, Daibosatsu, SQ-51, Toba OTT, TARA allanite) with variable elemental compositions and common lead concentrations have been used. Allanites with variations in FeO (from 12.8 to 16.1 wt%) and similar ThO_2 contents (around 1–2%) do not show significant matrix effects, as suggested by a previous study. While, obvious changes in calibration parameters (UO_2^+/U^+, ThO_2^+/Th^+) were noticed for allanites with a large range of Th contents (from 300 ppm to 2.0 wt%). By employing power law relationships between Pb^+/U^+ *versus* UO_2^+/U^+, Pb^+/Th^+ *versus* ThO_2^+/Th^+ with suitable exponentials, we do not observe obvious matrix effects with ThO_2 concentrations variations. This study demonstrates that allanite can be a good geochronometer for multi-stage mineralization of hydrothermal deposits, providing valuable complementary information to zircon and monazite.

Received 13th December 2019
Accepted 6th January 2020

DOI: 10.1039/c9ja00426b

rsc.li/jaas

Published on 07 January 2020. Downloaded on 1/14/2020 12:53:11 PM.

1. Introduction

Allanite [$(Ca,REE,Th)_2(Fe^{2+},Al)_3Si_3O_{12}(OH)$] is a common LREE-bearing mineral in the continental crust, defined by Giere and Sorenson[1] with REE + Th content ≥ 0.5 atoms per formula unit (apfu), or CaO content < 20 wt%. As an epidote-group mineral, allanite has varied elemental and isotopic compositions, predominantly controlled by the crystallization environment (*e.g.* melt/fluid[2,3]). Allanite usually incorporates a high concentration of Th and moderate amounts of U into its crystal structure, which gives it potential for a useful U–Th–Pb chronometer despite its tendency to incorporate non-negligible levels of common Pb. Compared with other minerals suitable for U–Pb chronology, allanite can crystallize in a wider range of P–T conditions. This property is presumably due to its compositional variability and propensity to incorporate substantial trace elements.[1,4] For example, allanite occurs in most granites and pegmatites like zircon and monazite, but also in different types of mid-low grade metamorphic rocks and hydrothermal deposits.[2,5,6] Hence allanite could be a good geochronometer and supply complementary information to zircon and monazite.

Previous studies have been conducted on dating allanite using isotope dilution methods,[7–9] but in some cases, these results are inaccurate due to compositional and textural complexities. *In situ* analyses have also been conducted by LA-ICP-MS and ion microprobe to eliminate the intricate pretreatment processes and avoid the altered or damaged zones.[10–13] Normally, the ion microprobe method has potential to achieve a better spatial resolution and precision over LA-ICP-MS when applied to complex geological processes like multi-stage mineralization. There were different understandings about matrix effect during SIMS allanite Th–Pb dating. Catlos, *et al.*[10] conducted allanite Th–Pb dating using a CAMECA IMS 1270 and suggested a significant matrix effect due to the variation of Fe concentrations. In contrast, Gregory, *et al.*[11] performed a similar investigation using SHRIMP and concluded that no matrix effects were induced by Fe contents on Th–Pb ages. Moreover, there was no discussion about matrix effects because of variations in Th and U contents.

[a]State Key Laboratory of Lithospheric Evolution, Institute of Geology and Geophysics, Chinese Academy of Sciences, Beijing, 100029, China. E-mail: liqiuli@mail.iggcas.ac.cn
[b]College of Earth and Planetary Sciences, University of Chinese Academy of Sciences, Beijing 100049, China
[c]Innovation Academy for Earth Science, Chinese Academy of Sciences, Beijing, 100029, China
[d]Swedish Museum of Natural History, Box 50007, SE-104 05 Stockholm, Sweden

† Electronic supplementary information (ESI) available. See DOI: 10.1039/c9ja00426b

Published on 07 January 2020. Downloaded on 1/14/2020 12:53:11 PM.

In this contribution, we performed U–Th–Pb measurements by using a CAMECA IMS 1280HR on five allanite samples with significant Fe and Th variation. We confirmed the insignificant matrix effects about Fe variation by SIMS, but also evaluated the possible matrix effects induced by Th variation. Additionally, it is noticed that allanite from hydrothermal deposit shows features of high U but low Th and very low common Pb, and could record multiple mineralization stages while zircon and monazite failed.

2. Sample descriptions

Five allanite samples were collected from different localities and rock types. They show different ages and a wide variation of chemical composition, which is suitable to test the potential matrix effects during SIMS analyses.

2.1 TARA

The Tara allanites crystallized in a granodiorite from the Berridale Batholith, southeast Australia. The allanite grains are 100–400 μm in diameter, gray in color, and usually have non-allanite components distributed at their outer margin. The BSE (backscatter electrons) images combined with compositional information show little compositional variation in a single crystal.[11] This granodiorite also contains zircon, titanite and apatite. Williams *et al.*[14] reported 412.0 ± 1.4 Ma biotite Rb–Sr and K–Ar ages as the emplacement time of Berridale pluton, which is consistent with the SHRIMP zircon U–Pb age of 418.7 ± 4.2 Ma within uncertainties.[15] ID-TIMS analyses performed on six grains of TARA allanites yielded a poorly defined lower intercept U–Pb age of 406.7 ± 8.2 Ma (MSWD = 83) on Tera–Wasserburg plot,[9] suggesting a possible radiogenic Pb loss. The *in situ* analytical results including allanite SHRIMP Th–Pb age of 414.9 ± 3.3 Ma and LA–ICP–MS Th–Pb isochron age of 414.4 ± 6.2 Ma, are consistent with each other and the emplacement age within uncertainties.[11] The discordance between whole grain and *in situ* analyses may reflect that the internal part of TARA allanite crystal keeps a close Th–Pb system, while the outer margin of crystal experienced Pb loss.

2.2 CAP

The CAP allanite originates from the Cima D'Asta Pluton granodiorite, South Alpine domain, Italy. It was regarded as the best alternative to zircon to constrain the emplacement age due to the overprinted hydrothermal activity. ID-TIMS analyses performed on four allanite grains yield a weighted average $^{208}Pb/^{232}Th$ age of 275.5 ± 1.5 Ma.[16] No open-system behavior of the Th–Pb age has been observed. The whole rock REE contents and Sm–Nd isotopic signatures also remain virtually unaffected, though a post-emplacement hydrothermal event exists. This CAP allanite Th–Pb age has been well reproduced by using another standard and hence CAP allanite has also been used as a well-established dating standard.[10,11,17]

2.3 TOBA

The Toba caldera complex, located in northern Sumatra, Indonesia, consists of four overlapping calderas erupted over the past 1.2 million years. The chronological line has been established from the ~1.2 Ma ~35 km^3 Haranggaol Dacite Tuff, the 0.84 ± 0.03 Ma ~500–2300 km^3 Oldest Toba Tuff (OTT), and the 0.501 ± 0.005 Ma >60 km^3 Middle Toba Tuff (MTT) to the ~74 Ma 2800 km^3 Youngest Toba Tuff (YTT).[18–22] The Toba allanite used in this paper was separated from a sample collected from the Toba OTT area. The characters of gray-color, clean-surface and relative small size (most <200 μm diameter) revealed from BSE image indicate that these grains are products of fast crystallization and least-affected by later hydrothermal and metamorphic events. Vazquez and Reid[23] demonstrated that most of allanites have identical ages with the eruption event, except that the core of a few large allanites are 0.025–0.15 Ma older than the eruption age. An Ar–Ar age of 0.84 ± 0.03 Ma was reported as the eruption age of Oldest Toba Tuff (OTT),[19] and also suggested as the reference age of OTT allanite with diameter of 100–300 μm.

2.4 Daibosatsu

The allanites, which occur as coarse-grained black prismatic crystals in a ~13 Ma granitic pegmatite, Daibosatsu Pass, Yamanashi, Japan, crystallized with quartz and a few plagioclases. Being enclosed by quartz shields these allanites from post-crystallization alteration and metamorphism. Back-scattered-electron images and X-ray element maps of the allanites show these crystals have chemically homogeneous distribution of major elements.[24] The previous application of this allanite was being used as a secondary standard to check the accuracy of *in situ* $^{143}Nd/^{144}Nd$, $^{147}Sm/^{144}Nd$, and Eu.[25] There are no isotopic constraints on the crystallization age of this allanite.

2.5 SQ-51

This allanite sample is from The Sin Quyen deposit in the Phan Si Pan belt of northwestern Vietnam. The deposit contains abundant Fe, Cu and REE, with subordinate Au and U. Ore bodies in this deposit are hosted in Proterozoic metapelite, and mainly consist of massive and banded replacement ores. The SQ-51 allanite grains are 100–300 μm in diameter. Few inclusions, inconspicuous compositional zoning and a clean surface can be observed in the BSE images. Hydrothermal zircon and monazite have been dated as similar U–Pb ages of 841 ± 12 and 834 ± 18 Ma, respectively. These ages were interpreted as the timing of the main Fe–REE–(U) mineralization stage at the Sin Quyen deposit.[26] The Cu–Au mineralization was considered as a later event after the Fe–REE mineralization stage by geological observations.[26] There is no time constrain about the Cu–Au mineralization stage till now.

3. Analytical procedure

The allanite samples were separated and cast into three 25 mm resin mounts with TARA allanites as standard since we collected them from different institutes at different times. The mounts were then polished to expose the internal sections of grains. The BSE images, major element compositions and SIMS U–Th–Pb dating were done at the Institute of Geology and Geophysics, Chinese Academy of Sciences (IGG-CAS).

 This journal is © The Royal Society of Chemistry 2020

Published on 07 January 2020. Downloaded on 1/14/2020 12:53:11 PM.

Allanite grains were imaged by backscattered electrons (BSE) using a scanning electron microscope. Major element compositions were obtained using a JEOL-JAX8100 electron microprobe with a 15 keV accelerating potential and 12 nA beam current, 5 μm beam spot, and 10–30 s counting time on different peaks. High-precision EPMA (Electro-Probe Micro-analyzer) analysis were implemented for (1) avoiding altered and chemically anomalous domains, (2) determining the compositional differences between different samples, (3) testing the accuracy of SIMS Th and U composition measurements.

After EPMA analysis, the sample mounts were coated with about 30 nm of high-purity gold to reach <20 Ω resistance. U–Th–Pb analyses were performed using the Chinese Academy of Sciences Cameca IMS-1280HR (CASIMS) at IGG-CAS. Three sessions have been conducted on three different mounts, *i.e.* TARA and CAP in session 1, SQ-51 and Daibosatsu in session 2 with TARA as standard, Toba and TARA allanites in session 3, respectively. The O_2^- primary ion beam was accelerated at 13 kV with intensity between 3–10 nA in different sessions. The aperture illumination mode (Kohler illumination) was used with a 200 μm primary beam mass filter (PBMF) aperture to produce even sputtering over the entire analyzed area. The ellipsoidal spot is about 20 × 30 μm in size. Positive secondary ions were extracted with a 10 kV potential. The $^{139}La^{28}Si^{16}O_2^+$ peak at mass 199 was used as a matrix signal. The ThO_2^+ peak was used as a reference peak for centering the secondary ion beam, energy and mass adjustments. The instrument was operated in high transmission (field aperture = 6000, maximum area = 40). Rectangular lenses were activated in the secondary ion optics to increase the transmission at high mass resolution. A mass resolution of *ca.* 7000 (defined at 50% peak height) was used, which is enough to separate U, Th, and Pb isotopes from isobaric interferences, such as oxides of rare earth elements, except for ^{204}Pb which could be interfered by unresolvable $ThNdO_2^{2+}$. A single electron multiplier was used in ion-counting mode to measure secondary ion beam intensities by a peak-jumping sequence. Because of variable Th contents of allanite and thus variable intensities, the parameters of electron multiplier, such as high volts, threshold value, and dead time were carefully adjusted. Each measurement consisted of 7 cycles, and the total analytical time was *ca.* 12 min.

4. Calibration protocols

4.1 Th/U calibration

The Th/U ratio plays a fundamental role in calculating Th and U contents, correcting the excess ^{206}Pb in U–Pb age and distinguishing the genetic types of allanite. Assuming that both the Pb–U and Pb–Th isotopic systems in a mineral are concordant, the radiogenic $^{208}Pb/^{206}Pb$ for the analyzed domain is related to the local $^{232}Th/^{238}U$ by:

$$\frac{^{208}Pb^*}{^{206}Pb^*} = \frac{^{232}Th(e^{\lambda_{232}t-1})}{^{238}U(e^{\lambda_{238}t-1})} \quad (1)$$

where λ_{232} is the ^{232}Th decay constant (4.9475×10^{-11} per year) and λ_{238} is the ^{238}U decay constant (1.55125×10^{-10} per year).[27] For a mineral standard, the $(e^{\lambda_{232}t-1})/(e^{\lambda_{238}t-1})$ is a constant depending on the corresponding age. The calculated $^{232}Th/^{238}U$ ratio could be determined by the equation mentioned above and approximately regarded as the Th/U ratio of the measured area. The coefficient between the calculated Th/U and measured Th/U-related ratios (such as ThO^+/UO^+ or ThO_2^+/UO_2^+) can be determined *via* the analytical data of a standard, and would be applied to the Th/U ratio calculation of unknown samples.

The correlation between measured Th_2O^+/U_2O^+ and calculated $^{232}Th/^{238}U$ in Tara data is illustrated in Fig. 1. A slope of 3.39 between Th_2O^+/U_2O^+ and Th/U is obtained with a correlation coefficient of 0.988. Consequently, the allanite Th/U ratios of unknowns were calculated using a linear relationship given by $Th/U = 3.39 \times Th_2O^+/U_2O^+$.

4.2 Calibration of U, Th concentrations

The most efficient way to determine the element abundances is to correct the corresponding ion counts by assuming a consistent ion yield. According to the EPMA-based Th contents and Th^+ counts data, the Daibosatsu allanite has most homogeneous Th content among these samples. The Th^+ ion yield is calculated as 1.40 cps ppm^{-1} nA^{-1} based on Daibosatsu allanite data. Then this value was used to determine the Th content of unknowns. The U contents were calculated from Th/U, which is generally calculated from ThO_2^+/UO_2^+ ($Th/U = 3.39 \times Th_2O^+/U_2O^+$ in allanite).

The best approach to test the accuracy of this calculating method is to compare the analyzed average Th content from EPMA and the calculated average Th concentration from SIMS data instead of comparing the single-spot data due to the different analyzed position and volume. The good agreement between analyzed average EPMA-based Th content and calculated average SIMS-based Th concentration from different samples demonstrates the reliability of the calculation procedure (ESI Fig. 1†).

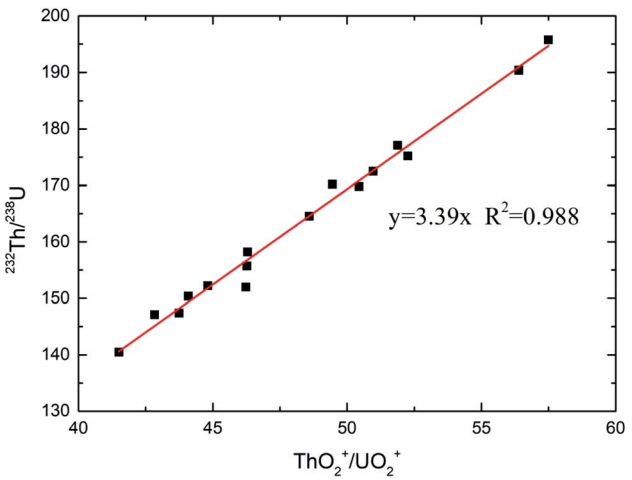


Fig. 1 Linear regression of the calculated Th/U *versus* Th_2O^+/U_2O^+ from TARA allanite analyses.

Published on 07 January 2020. Downloaded on 1/14/2020 12:53:11 PM.

4.3 Pb/U and Pb/Th calibration for allanite

There has been an obvious inter-elemental fractionation between Pb and U/Th, which means the observed Pb^+/U^+ and Pb^+/Th^+ ratios are inaccurate. The ratio, $^{206}Pb^+/^{238}U^+_{meas}/^{206}Pb/^{238}U_{true}$ clearly demonstrates this matrix dependence, for example, 2–4 times for zircon,[28] 30–60 times for perovskite,[29] 8–170 times for rutile,[30] 0.5–0.8 times and 7–10 times for baddeleyite with and without oxygen flooding, respectively.[31] In this study, the TARA allanite, which has the best reproducibility of U/Th–Pb ages, proper Th(U) and radiogenic Pb contents among the dated allanite samples, is used as the U/Th–Pb dating standard. The measured $^{206}Pb^+/^{238}U^+$ and $^{208}Pb^+/^{232}Th^+$ values of allanite are usually 30–160 times and 20–40 times higher than the true values, respectively. In consideration of distinct calibration approaches used by different researchers or carried on various minerals,[32,33] the power law $[^{206}Pb^+/^{238}U^+ = A \times ([UO_x]^+/^{238}U^+)^E]$ and $[^{208}Pb^+/^{232}Th^+ = A \times ([ThO_x]^+/^{232}Th^+)^E]$ should be the best choice and has been widely verified for U/Th–Pb dating on many minerals by ion microprobe analyses. The $^{206}Pb^*/^{238}U$ and $^{208}Pb^*/^{232}Th$ of an unknown sample can be calibrated as:

$$\frac{\frac{^{206}Pb^*}{^{238}U}_u}{\frac{^{206}Pb^*}{^{238}U}_{st}} = \frac{\frac{^{206}Pb^{*+}}{^{238}U^+}_u}{\frac{^{206}Pb^{*+}}{^{238}U^+}_{st}} = \frac{\frac{^{206}Pb^{*+}}{^{238}U^+}_u}{A\left(\frac{^{238}U_x^+}{^{238}U^+}\right)^E_u} \quad (2)$$

$$\frac{\frac{^{208}Pb^*}{^{232}Th}_u}{\frac{^{208}Pb^*}{^{232}Th}_{st}} = \frac{\frac{^{208}Pb^{*+}}{^{232}Th^+}_u}{\frac{^{208}Pb^{*+}}{^{232}Th^+}_{st}} = \frac{\frac{^{208}Pb^{*+}}{^{232}Th^+}_u}{A\left(\frac{^{232}ThO_x^+}{^{232}Th^+}\right)^E_u} \quad (3)$$

where u denotes the unknowns; * denotes radiogenic Pb and $x = 1$ or 2. The $^{206}Pb^*/^{238}U$ and $^{208}Pb^*/^{232}Th$ ratio of the TARA standard is calculated by the radiogenic function of $e^{\lambda t-1}$, where λ is the decay constant of ^{238}U and ^{232}Th, respectively. And t (= 412 Ma) is the reference age given by Williams *et al.*[14] On the log–log plot (*e.g.* Fig. 2), the exponential E is the slope and ln A is the intercept.

Previous studies[10] have illustrated that the secondary ion energy distributions of Pb^+ are more similar to the distributions of ThO_2^+ and UO_2^+ than those of ThO^+ and UO^+, indicating a better calibration to be achieved by ThO_2^+ and UO_2^+ criteria. Moreover, the ThO^+ has much higher ion yield than ThO_2^+. Thus, the ThO^+ counts of allanite more commonly do harm to ion counting electron multiplier (EM) than ThO_2^+, which will generate inaccurate data and cause premature detector aging. By employing the calibrating criteria of ThO_2^+/Th^+ and UO_2^+/U^+, slopes of 1.09 and 1.04 were recommended for Pb*/Th and Pb*/U correction based on the linear relationships from TARA measurements, respectively (Fig. 2).

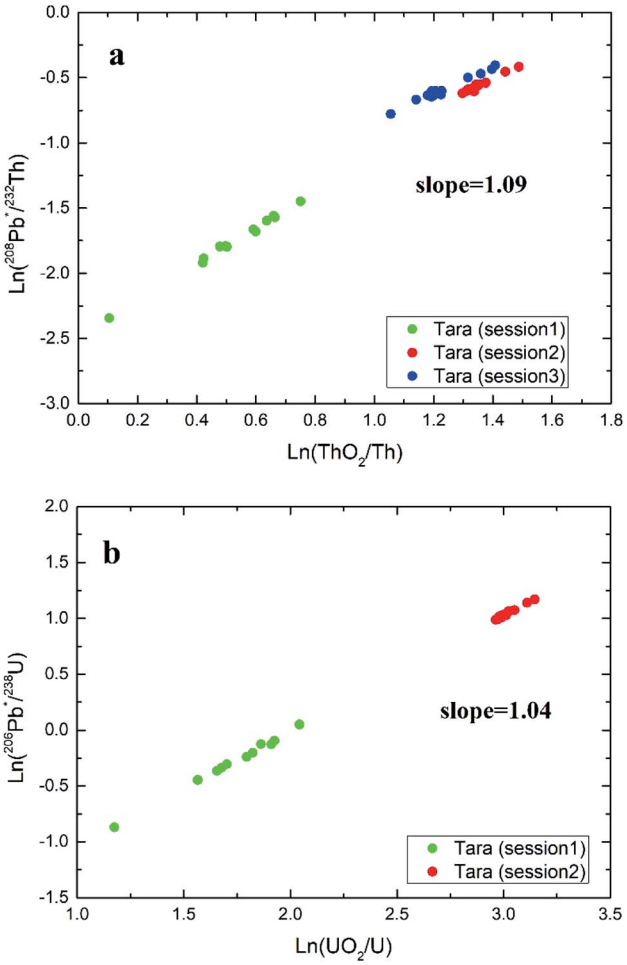


Fig. 2 Inter-elemental calibration diagrams of TARA allanites: (a) plot of secondary $\ln(^{208}Pb^{*+}/^{232}Th^+)$ *versus* $\ln(ThO_2^+/Th^+)$ ratios for TARA standard analyses; (b) plot of secondary $\ln(^{206}Pb^{*+}/^{238}U^+)$ *versus* $\ln(UO_2^+/U^+)$ ratios for TARA standard analyses.

4.4 Common Pb correction

For most minerals with low common Pb and relative high U (Th) contents like zircon and baddeleyite, a ^{204}Pb-based correction method is most frequently-used and effective. However, allanite has a propensity to incorporate large and variable amounts of non-radiogenic Pb into its crystal structure (called common lead), challenging the accuracy and precision of U–Th–Pb dating. Therefore, different common Pb correction approaches should be applied to specific samples. According to this study, the samples could be separated into three types: (1) Phanerozoic high-Th allanites without significant excess ^{206}Pb, (2) high-U and low common Pb allanite, (3) high-Th allanites with considerable excess ^{206}Pb.

For allanites with a relative high common Pb fraction ($^{206}Pb^+/^{204}Pb^+$ or $^{208}Pb^+/^{204}Pb^+ < 1000$), a ^{207}Pb-based correction is used. This correction is calculated by assuming U–Pb concordance and choosing a suitable common Pb composition. The "suitable common Pb composition" mentioned above can be estimated by projecting a regression line with the common Pb uncorrected data on a Tera–Wasserburg plot (for convenient, T–W are used below) or assuming the ratios from the "SK" model (the widely used two-stage terrestrial Pb evolution model of Stacey and Kramers[34]). The f_{206} value (the proportion of common ^{206}Pb in total ^{206}Pb) is calculated as:

Published on 07 January 2020. Downloaded on 1/14/2020 12:53:11 PM.

$$f_{206} = \frac{^{206}Pb_c}{^{206}Pb_T} = \frac{\frac{^{207}Pb}{^{206}Pb_m} - \frac{^{207}Pb^*}{^{206}Pb}}{\frac{^{207}Pb}{^{206}Pb_c} - \frac{^{207}Pb^*}{^{206}Pb}} \quad (4)$$

where $^{207}Pb/^{206}Pb_m$ is the measured ratio, $^{207}Pb^*/^{206}Pb^*$ is the radiogenic ratio for the inferred age and $^{207}Pb/^{206}Pb_c$ is the common Pb composition. It is applicable to Phanerozoic samples since the variation of $^{207}Pb^*/^{206}Pb^*$ is small. For Th–Pb system, f_{208} is calculated from:

$$f_{208} = f_{206} \times \frac{\frac{^{208}Pb}{^{206}Pb_c}}{\frac{^{208}Pb}{^{206}Pb_m}} \quad (5)$$

In case of allanites with low common Pb contents and relative high U (Th) contents, the ^{204}Pb-based correction method may be applied. The $^{204}Pb^+$ signals can be interfered by $^{144}Nd^{232}Th^{16}O_2^{2+}$. While, a relationship between intensities of $^{204}Pb^+$ and ThO_2^+ should be concerned before using this method during SIMS analyses on minerals containing abundant Th and LREE contents, such as monazite and allanite. Concerning the relatively invariable Nd contents in allanite, the ^{204}Pb-based correction method will be used if there is no positive relationship between ThO_2^+ and $^{204}Pb^+$. In present study, the samples containing 1% or higher Th contents are not suitable due to the obvious positive relationship between ThO_2^+ and $^{204}Pb^+$ (Fig. 3).

For a number of young allanites with high Th/U ratio, the excess initial ^{230}Th makes ^{207}Pb-based method impracticable due to the excess ^{206}Pb. Additionally, the U–Pb ages of these allanites are just recommended as an evaluation of concordance due to the higher common Pb concentration and uncertainty of excess ^{206}Pb. Fortunately, young samples with low U have almost negligible radiogenic ^{207}Pb. It is reasonable to regard the $^{207}Pb^+$ signals as all non-radiogenic, and then a Th–Pb isochron and an average Th–Pb age based on the ^{207}Pb correction method can be constructed. So the f_{208} is calculated from:

$$f_{208} = \frac{^{208}Pb_c}{^{208}Pb_T} = \frac{^{208}Pb}{^{207}Pb_c} \times \frac{^{207}Pb^+}{^{208}Pb^+} \quad (6)$$

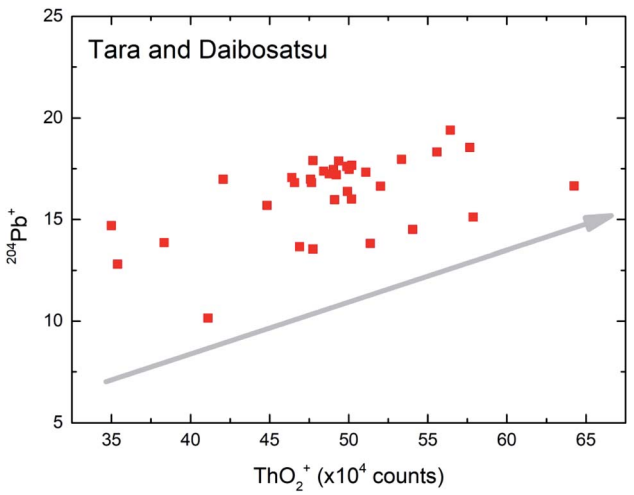


Fig. 3 Plot of ThO_2^+ *versus* $^{204}Pb^+$ indicating the interference of $^{232}Th^{144}Nd^{16}O_2^+$ on $^{204}Pb^+$, the Tara and Daibosatsu measurements were conducted in a same session.

4.5 Excess ^{206}Pb from ^{230}Th

Since the Th/U ratio in allanite is commonly higher than the Th/U ratio in whole rock, the excess ^{206}Pb derived from the decay of initial excess ^{230}Th must be deducted to derive the correct $^{206}Pb/^{238}U$ age. The excess ^{206}Pb can be corrected by:

$$\Delta \frac{^{206}Pb}{^{238}U} = \left[\frac{\lambda_{238}}{\lambda_{230}}(f-1) \times \frac{1}{e^{\lambda_{238}t} - 1}\right] \times 100\%,$$

therein

$$f = \frac{\frac{^{232}Th}{^{238}U}_{allanite}}{\frac{^{232}Th}{^{238}U}_{magma}}$$

and Δ is the proportion of ^{206}Pb decayed from ^{230}Th over the $^{206}Pb^*$ rather than $^{206}Pb_T$.

5. Results

The results of EPMA and SIMS U–Th–Pb dating are listed in ESI Tables 1 and 2,† respectively. The U–Th–Pb decay constants used in age processing are quoted from Steiger and Jäger[27] and the calculation routines of Isoplot/Ex.[35] The resulting regressions and weighted average ages are quoted at the 95% confidence interval.

5.1 TARA

Based on EPMA measurements, the FeO content of TARA are relatively homogeneous with an average at 14.4 ± 0.6 wt% (ESI Table 1†). The ThO_2 contents vary from 0.68 to 1.52 wt% (ESI Table 1†). The SIMS measurements show that the Th contents of TARA vary from 4000 ppm to 1.6 wt% and the U contents calculated from Th contents and Th/U ratio range from 30 to 220 ppm (ESI Table 2†). The external reproducibility of TARA U–Pb and Th–Pb ages in session 1 and session 2 were 1.31% and 1.31%, 0.73% and 0.98% (ESI Table 2†), respectively. Only Th–Pb dating was conducted in session 3 to yield an external reproducibility of 1.43% for TARA (ESI Table 2†). The relatively low common Pb concentration ($f_{206} \sim 7$–20% and $f_{208} < 1\%$) and good U/Th–Pb age reproducibility demonstrate its applicability as a U–Th–Pb dating standard.

5.2 CAP

Ten EPMA measurements exhibit FeO contents ranging from 10.2 to 14.0 wt%, ThO_2 contents of 0.96 to 2.31 wt% (ESI Table 1†). Twenty SIMS analyses were conducted on CAP grains. Based on SIMS analyses, these allanites contain Th contents of 7000–

Published on 07 January 2020. Downloaded on 1/14/2020 12:53:11 PM.

17 000 ppm, U of 50–350 ppm and Th/U of 40–170 (ESI Table 2†). Except two outliers, 18 of them yield a weighted average Th–Pb age of 275.0 ± 4.3 Ma and U–Pb age of 278.4 ± 2.5 Ma corrected by ^{207}Pb-based method (Fig. 4a). The lower intercept of 277.6 ± 6.0 Ma illustrated in T–W diagram is also consistent with the reference ages (Fig. 4a).

5.3 TOBA OTT

Toba allanite is a group of young minerals with FeO contents of 15.1–17.0 wt% and ThO_2 contents of 1.0–2.7 wt% (ESI Table 1†) based on EPMA analyses. A total of 20 SIMS analyses on 20 grains show that the f_{208} values are homogeneous and averaged at 0.69 ± 0.02 (ESI Table 2†). The error of a single-spot age is propagated from the age reproducibility of the standard, statistical error of $^{208}Pb^{+}/^{232}Th^{+}$ ratio and the assigned error of common Pb composition. A weighted average Th–Pb age of 0.83 ± 0.04 Ma (MSWD = 0.16) is consistent with an isochron age of 0.84 ± 0.06 Ma (n = 20, MSWD = 1.7) (Fig. 4b).

5.4 Daibosatsu

EPMA data from ten grains shows homogenous FeO contents with an average of 15.9 ± 0.1 wt% (ESI Table 1†). There were 20 SIMS measurements made on Daibosatsu allanites and only one of them was excluded due to non-allanite composition. These grains contain comparatively homogeneous Th and U contents and Th/U ratios, *i.e.* 1.05 ± 0.07 wt%, 230 ± 9 ppm and 45.7 ± 1.9 (2 SD, ESI Table 2†), respectively. By regarding the $^{207}Pb^{+}$ signals as all non-radiogenic, a weighted average Th–Pb age of 11.5 ± 0.2 Ma is yielded (Fig. 4c). A free regression line on a T–W plot produced a U–Pb age of 9.3 ± 3.0 Ma due to their high common Pb and rather clustered distribution (Fig. 4c).

5.5 SQ-51

The EPMA data show that the average FeO content is 15.0 ± 0.4 wt% (ESI Table 1†), and Th content is below the detection limit. Twenty analyses were conducted on SQ-51 particles by SIMS analyses. The U contents vary from 800 to 1600 ppm and Th contents range from 250 to 300 ppm (ESI Table 2†). These grains differ from other samples in their extremely low common Pb contents ($^{206}Pb/^{204}Pb$ > 10 000) and low Th/U ratios (<1). By virtue of the low common lead proportion and rather older age, high precision $^{207}Pb/^{206}Pb$ ages were achieved, which can be separated into two groups. The main group consists of 17 grains yielding a weighted average $^{207}Pb/^{206}Pb$ age of 779.3 ± 3.7 Ma (n = 17, MSWD = 0.45, Fig. 5b). Except one point showing obvious Pb loss, sixteen analyses of the main group show a weighted average $^{206}Pb/^{238}U$ age of 771.0 ± 3.1 Ma (n = 16, MSWD = 0.87) and a weighted average $^{208}Pb/^{232}Th$ age of 778.3 ± 9.2 Ma (n = 16, MSWD = 2.6) (Fig. 5b). The rest three measurements of another group show Pb–Pb ages above 830 Ma and slight Pb loss. The older group includes three points with a mean $^{207}Pb/^{206}Pb$ age of 835 ± 9 Ma (n = 3, MSWD = 0.98), $^{206}Pb/^{238}U$ ages of 816–837 Ma, $^{208}Pb/^{232}Th$ ages of 822–831 Ma.

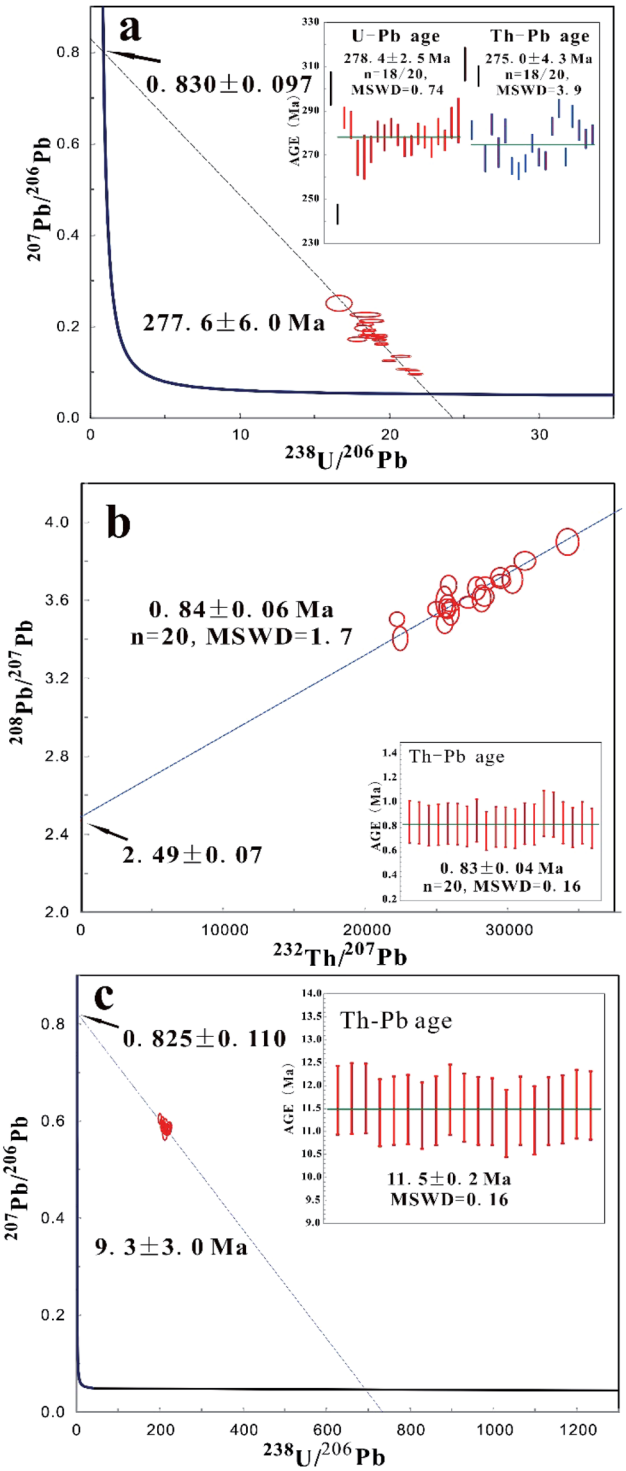


Fig. 4 Age results of allanite samples. (a) CAP measurements plotted in Tera–Wasserburg diagram with weighted average U–Pb and Th–Pb ages inserted; (b) TOBA Th–Pb isochron age with weighted average Th–Pb age inserted; (c) Daibosatsu measurements plotted in Tera–Wasserburg diagram with weighted average Th–Pb age inserted. Data point error bars and weighted average age uncertainties are at 2σ level.

This journal is © The Royal Society of Chemistry 2020

Published on 07 January 2020. Downloaded on 1/14/2020 12:53:11 PM.

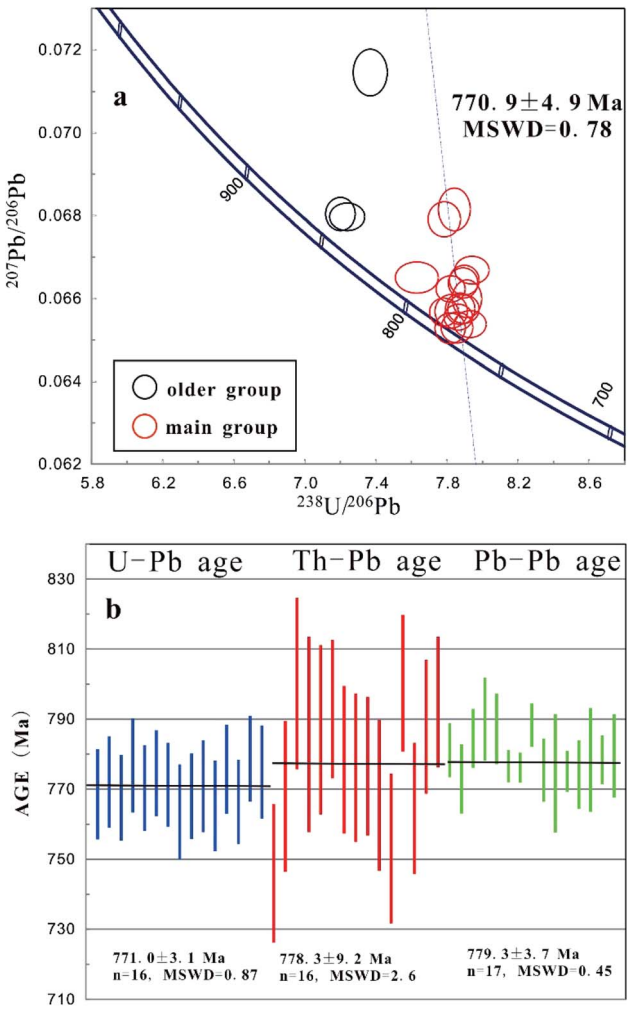


Fig. 5 Age results of SQ-51 allanites. (a) SQ-51 measurements plotted in Tera–Wasserburg diagram. (b) Weighted average U–Pb, Th–Pb and Pb–Pb ages for the main group. Data point error bars and weighted average age uncertainties are at 2σ level.

6. Discussion

6.1 Age validity and matrix effect

For evaluation of SIMS age results, the common approach is to compare the corrected age with the corresponding reference age. By applying the calibration protocols, the final age results are summarized in Table 1 with reference ages and two critical matrix criteria (Th, FeO contents). The average U–Pb and Th–Pb ages of CAP sample are consistent with the TIMS results within uncertainties.[16] The average Th–Pb age and Th–Pb isochron age of TOBA allanites are consistent with eruption age inferred from Ar–Ar dating.[19] This observation agrees well with previous investigation, *i.e.* most of allanites have identical ages with the eruption event.[23] There is no precise age constraint on Daibosatsu allanites. Only a rough age of ~13 Ma was recommended as the time of the host granitic pegmatite.[25] Considering that the allanite Th–Pb age normally constrains the late stage of magma as TOBA allanites do, the 1.5 Ma age gap between our new Th–Pb age of 11.5 ± 0.2 Ma and this recommended ~13 Ma rock age could be reasonable or may do not exist. It could not be solid evidence used to discuss the age validity and matrix effects. As for the SQ-51 allanites from Sin Quyen deposit, two age populations were well determined by Pb–Pb ages. The older group of allanites (835 ± 9 Ma) are in good agreement with the hydrothermal zircons and monazites reported in the same deposit.[26] The majority of allanites yield the consistent U–Pb and Th–Pb ages with the corresponding Pb–Pb ages, indicating the age validity and close U–Th–Pb system. To sum up, our analytical protocol without matrix effect correction works well for these test samples (ESI Fig. 2†).

For SIMS analyses, different elements have different secondary ionization efficiencies and different propensities to form multiple oxides. Even if the target is chemically homogeneous, the measured secondary ion ratios not only differ substantially from the isotope ratios in the target, but those ion ratios also change during a SIMS analysis.[36] The Pb^+/U^+ and UO^+/U^+ or UO_2^+/U^+ (and Pb^+/Th^+ *vs.* ThO^+/Th^+ or ThO_2^+/Th^+) have been found as co-varying pairs for a target with constant Pb/U, and have become the basis for SIMS U–Th–Pb calibration procedures. The proportional relationship between standard and unknowns (eqn (2) and (3)) must be used with same UO^+/U^+ or UO_2^+/U^+ (or ThO^+/Th^+ and ThO_2^+/Th^+) (for convenience, only ThO_2^+/Th^+ and UO_2^+/U^+ are used below). If the unknowns show quite different ThO_2^+/Th^+ (UO_2^+/U^+), an extension of calibration line would be used. Then the exponent in eqn (2) and (3) will be important. Unsuitable exponent would produce quite different age results and matrix effect will be suggested.

In present work, the TARA allanite standards in each session defined very close calibration curves (Fig. 2). The spreads of UO_2^+/U^+ and ThO_2^+/Th^+ are similar between allanite samples with high

Table 1 The summarized SIMS dating results with corresponding compositional variations

Sample	Th[a] (ppm)	FeO[b] (wt%)	Reference age (Ma)	$^{206}Pb/^{238}U$ age (Ma)	f_{206} (%)	$^{208}Pb/^{232}Th$ age (Ma)	f_{208} (%)	$^{207}Pb/^{206}Pb$ age (Ma)
Tara	7000–13 000	13.7–15.9	412.0 ± 1.4[c]	1.50%[d]	10–25	1.42%[d]	0.6–1.5	NA[e]
CAP	7000–16 000	10.6–14.0	275.5 ± 1.5[f]	277.6 ± 6.0	5–25	275.0 ± 4.3	0.7–1.7	NA
SQ-51	200–320	14.6–15.6	$^{207}Pb/^{206}Pb$ age	816–837	0.1–0.6	822–831	0.1–0.6	830–845
			$^{207}Pb/^{206}Pb$ age	771.0 ± 3.1		778.3 ± 9.2		779.3 ± 3.7
Daibosatsu	9000–12 000	15.7–16.0	No reference	9.3 ± 3.0	60–64	11.5 ± 0.2	20–26	NA
TOBA	15 000–20 000	15.1–17.0	0.84 ± 0.03[g]	NA	NA	0.84 ± 0.06	65–72	NA

[a] Elemental concentrations are calculated by SIMS data. [b] Elemental composition are quoted from EPMA data. [c] Referred from Williams *et al.* (1983).[14] [d] The percentage is extracted from the biggest standard deviation between three sessions. [e] NA = not analyzed. [f] Referred from Barth *et al.* (1994).[16] [g] Referred from Diehl *et al.* (1987).[19]

Published on 07 January 2020. Downloaded on 1/14/2020 12:53:11 PM.

Th contents (around 0.7–2 wt%) (Fig. 6a), but exhibit an obvious difference of SQ-51 with much lower Th concentrations (~260 ppm) (Fig. 6b). This phenomenon is quite similar to SIMS monazite dating.[33] Those samples with similar Th contents and therefore similar UO_2^+/U^+ and ThO_2^+/Th^+ range with Tara standard yielded consistent age results with reference ages. It indicates that no obvious matrix effects on allanite U–Th–Pb dating were observed with a range in FeO from 12.8 to 16.1 wt%. With the extension line as calibrated curve, SQ-51 with much lower Th than TARA standard also yielded consistent U–Pb and Th–Pb ages with corresponding independent Pb–Pb ages (except two spots with obvious radiogenic Pb loss). It suggests that no obvious matrix effects for allanite samples with ThO_2 from 300 ppm to 2.0 wt%.

6.2 Applications of allanite U–Th–Pb dating

The geological significance of an isotopic age is largely related to the relationship between crystallization temperature and closure temperature of the radioactive system. Oberli *et al.*[8] observed the preservation of excess ^{206}Pb in magmatic zoned allanites, which indicates that the isotopic systems have not been reset by loss of radiogenic Pb during prolonged residence at magmatic conditions. The results support closure temperature exceeding 700 °C. Such a high closure temperature makes allanite to potentially be a good geochronometer recording the time of crystallization. Additionally, inheritance (not only the inherited mineral, but also the inherited Pb isotope) in allanite is much less common than in zircon, though been reported,[3,37] presumably attributed to the lower temperatures of allanite saturation and of Pb diffusion through the allanite lattice.[9]

In general, allanite incorporates Th in preference to U. Previous *in situ* allanite dating mainly used the Th–Pb system due to its obvious advantage over the U–Pb system.[10] It is noteworthy that the combined information of Th–Pb and U–Pb ages is more credible than the Th–Pb system alone.[5,11,16] The deficiency on allanite geochronometer is a lack of least-affected Pb–Pb age because of usual high common Pb and the inapplicability of ^{204}Pb-based correction of high Th samples (interference by $ThNdO_2^+$). In the present work, we demonstrate that the U–Pb and Th–Pb ages can be simultaneously determined, allowing an internal examination of age concordance. Generally, the precision of allanite U–Pb age is substantially restricted by the low U content, high common Pb proportion and the presence of excess ^{206}Pb. Hydrothermal allanite, like SQ-51, is a particular case, *i.e.* containing high U but low Th and low common Pb. This kind of allanite is preferred to be dated by U–Pb system over Th–Pb system. Hydrothermal allanite can play a fundamental role in ore deposits dating since this common trace elements (LREE, Th, Sr) carrier is tightly connected with the ore-forming fluids. Additionally, the elemental and isotopic information excavated from the mineral, like REE–Th–U contents and the initial common Pb composition, could effectively reflect the characters and sources of the fluids. The older three spots (SQ-51@3,6,8, ESI Table 2†) which show consistent age with the monazites reported in the same deposit could be the evidence of multi-stage mineralization.[38] The lesser amounts of older allanite measurements probably are attributed to co-existing monazite. Monazite preferentially absorbs Th and REE elements into their crystals and then the formation of allanites would be restricted by the lack of those elements in the fluids.[3] Multi-stage crystallization has also been reported in which primary allanites contain higher REE contents and then be partly replaced by porous and REE-poor secondary allanites.[39] Consequently, precise U–Th–Pb and Pb–Pb ages, together with distinguishable characters of multi-stage allanites, could collectively be used for comprehensively assessing the accuracy and significance of the isotopic age and constraining the behaviour of allanites in a hydrothermal activity.

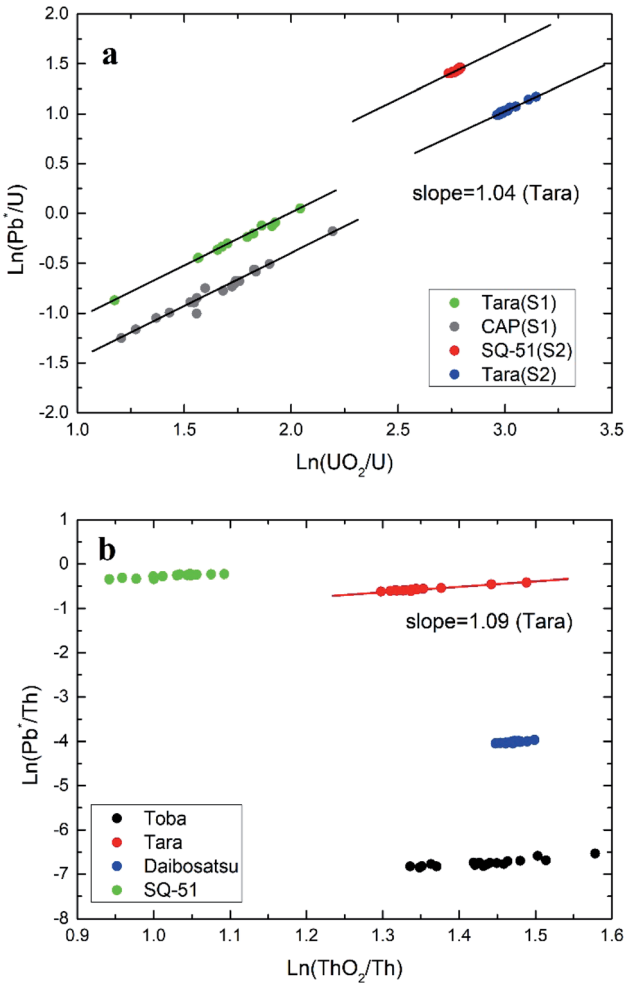


Fig. 6 Inter-elemental calibration diagrams. (a) Plot of $\ln(^{206}Pb^{*+}/^{238}U^+)$ *versus* $\ln(UO_2^+/U^+)$ ratios for TARA standard analyses, where S1 and S2 represent different analyzing sessions; (b) plot of $\ln(^{208}Pb^{*+}/^{232}Th^+)$ *versus* $\ln(ThO_2^+/Th^+)$ ratios for TARA standard analyses, where the $\ln(^{208}Pb^{*+}/^{232}Th^+)$ values of Toba measurements are corrected by the proportional relationship between TARA standard measurements in these two sessions.

7 Conclusions

(1) By applying power law relationships between Pb^+/U^+ *versus* UO_2^+/U^+, Pb^+/Th^+ *versus* ThO_2^+/Th^+ and suitable exponentials, SIMS U–Th–Pb dating on allanites with a range of FeO (from 12.8 to 16.1 wt%) and ThO_2 (from 300 ppm to 2.0 wt%) exhibit no obvious matrix effects.

This journal is © The Royal Society of Chemistry 2020

Published on 07 January 2020. Downloaded on 1/14/2020 12:53:11 PM.

(2) Allanite has a propensity to incorporate large and variable amounts of common Pb, challenging the accuracy and precision of U–Th–Pb dating. ^{204}Pb-based common lead correction method works well for low Th allanites, but would be problematic for high Th allanite. ^{207}Pb-based method is suitable for older sample without obvious excess ^{206}Pb. For young samples, $^{207}Pb^{+}$ can be regarded as all common Pb and used for common Pb correction for single-spot analyses or *via* an isochron regression method.

(3) The accuracy of allanite U–Th–Pb dating is predominantly controlled by the common Pb proportion (f_{206} and f_{208}). For Phanerozoic allanites with high Th and relative low common Pb ($f_{206} \sim 20\%$, $f_{208} < 1\%$), the precision of weighted average U–Pb and Th–Pb ages both can be achieved within 2% (at 95% confidence). For hydrothermal allanite with high U and low common Pb (f_{206}, $f_{208} < 1\%$), the precision can be better than 1.5% (at 95% confidence).

(4) Hydrothermal allanites in IOCG deposits has very low common Pb and high U, which simultaneously makes precise U–Pb, Th–Pb and Pb–Pb ages feasible. The dating results exhibit robust radioactive systems of multi-stage crystallized allanites. Allanite U–Th–Pb dating can potentially be applied to more hydrothermal deposits.

Conflicts of interest

There are no conflicts to declare.

Acknowledgements

We thank Ms H. X. Ma for preparing sample mounts, Mr Q. Mao for assisting with EPMA analyses. Engineers' efforts (Mr G. Q. Tang and Ms J. Li) on SIMS analyses are appreciated as well. Comments and suggestions by Prof. X. H. Li, Y. Li are greatly acknowledged. We also thank The China Scholarship Council (CSC) for supporting the author studying in Sweden for one year. This work was financially supported by the National Key R&D Program of China (2016YFE0203000), the National Nature Sciences Foundation of China (Grants no. 41525012, 41773044 and 41673059), and National Program for Support of Top-notch Young Professionals.

References

1 R. Giere and S. S. Sorensen, *Rev. Mineral. Geochem.*, 2004, **56**, 431–493.
2 B. A. Wing, J. M. Ferry and T. M. Harrison, *Contrib. Mineral. Petrol.*, 2003, **145**, 228–250.
3 R. L. Romer and S. Siegesmund, *Contrib. Mineral. Petrol.*, 2003, **146**, 297–307.
4 E. Janots, F. Negro, F. Brunet, B. Goffé, M. Engi and M. L. Bouybaouène, *Lithos*, 2006, **87**, 214–234.
5 E. Janots, M. Engi, D. Rubatto, A. Berger, C. Gregory and M. Rahn, *Geology*, 2009, **37**, 11–14.
6 K. R. Boston, D. Rubatto, J. Hermann, M. Engi and Y. Amelin, *Lithos*, 2017, **286**, 502–518.
7 V. Blanckenburg, *Chem. Geol.*, 1992, **100**, 19–40.
8 F. Oberli, M. Meier, A. Berger, C. L. Rosenberg and R. GierÉ, *Geochim. Cosmochim. Acta*, 2004, **68**, 2543–2560.
9 A. J. Smye, N. M. W. Roberts, D. J. Condon, M. S. A. Horstwood and R. R. Parrish, *Geochim. Cosmochim. Acta*, 2014, **135**, 1–28.
10 E. J. Catlos, S. S. Sorensen and T. M. Harrison, *Am. Mineral.*, 2000, **85**, 633–648.
11 C. J. Gregory, D. Rubatto, C. M. Allen, I. S. Williams, J. Hermann and T. Ireland, *Chem. Geol.*, 2007, **245**, 162–182.
12 J. R. Darling, C. D. Storey and M. Engi, *Chem. Geol.*, 2012, **292**, 103–115.
13 X. D. Deng, J. W. Li and G. Wen, *Chem. Geol.*, 2014, **382**, 95–110.
14 I. S. Williams, W. Compston and B. W. Chappell, *J. Petrol.*, 1983, **24**, 76–97.
15 R. B. Ickert and I. S. Williams, *Aust. J. Earth Sci.*, 2011, **58**, 501–516.
16 S. Barth, *Earth Planet. Sci. Lett.*, 1994, **124**, 149–159.
17 R. A. Cox, D. H. C. Wilton and J. Kosler, *Can. Mineral.*, 2003, **41**, 273–291.
18 M. D. Knight, G. P. L. Walker, B. B. Ellwood and J. F. Diehl, *J. Geophys. Res.*, 1986, **91**, 10355.
19 J. F. Diehl, *Geophys. Res. Lett.*, 1987, **14**, 753–756.
20 C. A. Chesner, *Geology*, 1991, **19**, 200–203.
21 C. A. Chesner, *Quat. Int.*, 2012, **258**, 5–18.
22 M. R. Reid and J. A. Vazquez, *Geochem. Geophys. Geosyst.*, 2017, **18**, 156–177.
23 J. A. Vazquez and M. R. Reid, *Science*, 2004, **305**, 991–994.
24 M. Hoshino, M. Kimata, N. Nishida, A. Kyono, M. Shimizu and S. Takizawa, *Mineral. Mag.*, 2005, **69**, 403–423.
25 C. R. M. McFarlane and M. T. McCulloch, *Chem. Geol.*, 2007, **245**, 45–60.
26 X.-C. Li, M.-F. Zhou, W. T. Chen, X.-F. Zhao and M. Tran, *Miner. Deposita*, 2018, **53**, 399–416.
27 R. H. Steiger and E. Jäger, *Earth Planet. Sci. Lett.*, 1977, **36**, 359–362.
28 R. A. Stern and Y. Amelin, *Chem. Geol.*, 2003, **197**, 111–142.
29 Q.-L. Li, X.-H. Li, Y. Liu, F.-Y. Wu, J.-H. Yang and R. H. Mitchell, *Chem. Geol.*, 2010, **269**, 396–405.
30 Q. L. Li, W. Lin, W. Su, X. H. Li, Y. H. Shi, Y. Liu and G. Q. Tang, *Lithos*, 2011, **122**, 76–86.
31 Q. L. Li, X. H. Li, Y. Liu, G. Q. Tang, J. H. Yang and W. G. Zhu, *J. Anal. At. Spectrom.*, 2010, **25**, 1107–1113.
32 I. R. Fletcher, N. J. McNaughton, W. J. Davis and B. Rasmussen, *Chem. Geol.*, 2010, **270**, 31–44.
33 Q. L. Li, X. H. Li, Z. W. Lan, C. L. Guo, Y. N. Yang, Y. Liu and G. Q. Tang, *Contrib. Mineral. Petrol.*, 2013, **166**, 65–80.
34 J. S. Stacey and J. D. Kramers, *Earth Planet. Sci. Lett.*, 1975, **26**, 207–221.
35 A. D. Anbar and A. H. Knoll, *Science*, 2002, **297**, 1137–1142.
36 T. R. Ireland, W. Compston, I. S. Williams and I. Wendt, *Earth Planet. Sci. Lett.*, 1990, **101**, 379–387.
37 C. J. Gregory, D. Rubatto, J. Hermann, A. Berger and M. Engi, *Geochim. Cosmochim. Acta*, 2012, **84**, 433–458.
38 X. C. Li and M. F. Zhou, *Am. Mineral.*, 2017, **102**, 1525–1541.
39 W. T. Chen and M. F. Zhou, *Contrib. Mineral. Petrol.*, 2014, **168**, 1043–1062.

View publication stats

ResearchGate

See discussions, stats, and author profiles for this publication at: https://www.researchgate.net/publication/338430167

Allanite U–Th–Pb geochronology by ion microprobe

Article *in* Journal of Analytical Atomic Spectrometry · January 2020

DOI: 10.1039/C9JA00426B

CITATIONS
0

READS
67

5 authors, including:



Liao Xin
Chinese Academy of Sciences
3 PUBLICATIONS **11** CITATIONS
SEE PROFILE



Yueheng Yang
Chinese Academy of Sciences
226 PUBLICATIONS **12,002** CITATIONS
SEE PROFILE

Some of the authors of this publication are also working on these related projects:

LA-(MC)-ICP-MS View project

Interaction models of crustal and mantle rocks with fluids in accretionary wedges of the Western Carpathians, eastern Alps and northern Turkey; correlation of P-T-X-t parameters View project

All content following this page was uploaded by Liao Xin on 15 January 2020.

The user has requested enhancement of the downloaded file.